Dear Prof. Edith Gallagher,

We wish to thank you for your constructive and positive comments that helped to improve the paper. We took into account all of them to write the revised version of our manuscript. Moreover, other changes have been made as suggested by the other reviewer.

The main changes concern (please see the new manuscript; italic font indicates new text, strikethrough font indicates old text):

- Section 2 (Field site and video imagery) restructured. We add section 2.3 (3-D geometry) and section 2.4 (Piecewise regression of the bar movement). Changes have been made in Fig. 8 (new manuscript).

- Section 4.2 renamed, restructured and shortened. Particularly, we removed the analysis of the wave energy flux (P, P_Y) as well as S_xy (Fig. 10 and Fig. 11 of the new manuscript have been simplified).

- Section 4.3 (Sediment transport) restructured, shortened and improved.

    - Section 4.3.1 (Soulsby and Van Rijn formula) describes the sediment transport formulation. The analysis by considering a constant wave stirring has been removed (Section 4.3 Sediment transport; Fig. 14).

    - Section 4.3.2 (Tidal correction factor). A new tidal correction factor is defined. In the previous version of the manuscript, we introduced a tidal factor that depends on the tidal range only. The new tidal correction factor depends on the hourly tidal level. Emphasis on this factor and details on its formulation have been given in the new section 4.3.2 (Tidal correction factor) with the help of two new figures (Fig. 12 and Fig. 13).

    - Section 4.3.3 (Results). The sediment transport has been averaged over the same time intervals as the bar migration (see red lines in Fig. 14)

- English errors. The two reviewers have indicated editorial/english errors that have been corrected.

Please find on the attached file our reply to your comments (blue font indicates your comments, black font indicates our answer) as well as the strongly version of our manuscript: “Intertidal finger bars at El Puntal, Bay of Santander, Spain: observation and forcing analysis” (italic font indicates new text, strikethrough font indicates old text).

We hope that the new manuscript will be evaluated positively.

Yours sincerely,

(on behalf of all authors)

Erica Pellón

GENERAL COMMENTS

This manuscript describes observations of small bedforms, referred to as finger bars, on the southern, sheltered side of the El Puntal spit, at the mouth of the Santander Bay. The observations are interesting (2 years of data from video cameras) and include orientation and migration of the finger bars. The extraction of bathymetry data using the shoreline of the rising and falling tide is a particularly elegant analysis (there should be more on the bathymetry obtained in this way, maybe a comparison with measurements to verify it). My biggest criticism is the lack of measurements of the fluid forcing on the bars, but without that I still think the paper is publishable. I feel that the paper needs some revisions, recalculation and some more explanation.

We thank you for these comments.

More emphasis has been given on the extraction of bathymetry data using the shoreline of the rising/falling tide, by including a new section (2.3 3-D geometry). As we explain in the new manuscript, the extraction of bathymetric data is subject to the meteorological conditions, which have to be excellent to obtain correct results. This extraction of bathymetric data using the shoreline has been done for 12 days but without as good results as the shown one.

A comparison with bathymetric measurement to verify such results is underway. Preliminary (over a small part of the bar system) performed by using a laser-scanner shows encouraging results, but we have decided to not include them as the measurement date does not coincide with the study period of the present analysis.

Measurement of the fluid forcing on the bar is also under planning and we hope this will be presented in a next contribution.

SPECIFIC COMMENTS

Comment 1: I wonder about the averaging time. I think that the season-long averages shown in figures 11 and 12 might be smoothing over important events or periods that contribute to the calculations of average bar migration. The bar migration is averaged over the different length chunks, which the authors state is about 70 days on average. It would make more sense to average the variables in Figs 11 and 12 over similar time periods to make them more comparable to the bar migration speeds. (Also the explanation of the calculation of V_k could use clarification.)

The explanation of the calculation of V_k has been improved in the manuscript by adding a new section (2.4 Piecewise regression of the bar movement). It describes the methodology followed to obtain the time-dependent migration rate (V_m). Notice that Fig. 8 has been modified to facilitate the understanding.

Furthermore, taking into account your suggestion, we have added in Fig. 12 (now it is Fig. 14) a new curve (red line), where the sediment transport has been averaged over the same time intervals as the bar migration. Now the correlation is performed by comparing the red and black lines (Fig. 14). This gives better results.

Comment 2: I think that adopting the Soulsby Van Rijn formulation with the wave-stirring factor is definitely better than the constant stirring approach. (In fact the calculation using the 'constant stirring model' is so poor as to not be worth showing.) Clearly tiny little waves like those are not going to be driving a significant alongshore current. I might go even further to not just parameterize wave-stirring effects, but try to look at the transport by wave orbital velocities. I'll bet those finger bars are driven by the small net transport associated with those tiny waves shoaling and breaking. As the tide rises and falls a little mini surf zone moves up and down the beach. In fact, I wonder if the curvature of the bars has to do with the little mini surf zone spending more time along those lower sections of the bars.

We agree with you, the constant wave stirring approach is not relevant here. We have decided to remove it (Section 4.3 shortened; Fig. 14 contains now 2 panels). Actually, the previous modelling studies which used this approach (e.g. Garnier et al., 2006) consider a fixed incident wave height during their simulations; this is not applicable here.

Concerning the transport by wave orbital velocities, we made different tests by including the sediment transport formula described in Garnier et al., 2007 (PhD Thesis), based on the study of Plant et al., 2001 (Plant, N.G., Ruessink, B.G. & Wijnberg, K.M., 2001, Morphologic properties derived from a simple cross-shore sediment transport model, J. Geophys. Res. 106, 945-962). The magnitude of this sediment transport is one order of magnitude less than the SVR transport. Furthermore, the use of this sediment transport formulation alone gives poor correlation with the bar migration speeds. For these reasons, this formulation has not been introduced in the new manuscript.

Concerning the mini surf zone moving up and down the beach, we have included this effect through the "tidal correction factor", see Comment 4 bellow.

Comment 3: Throughout the paper I was thinking that you needed to include time of submersion (high tide versus low tide). At the end you throw in the tidal factor, which is great, but your explanation is brief and I don't really know how you did it (and if it will capture the tidal effect). It clearly helps your results, but it would help the reader to know what is involved in that factor, since it is clearly important.

To take into account the different periods of time that the waves spend over the bars on each day, we introduced the tidal correction factor. In the first version of the manuscript, this factor depended on the tidal range, however, following your Comment 4 (see bellow), this factor depends now on the hourly varying tidal level. As a result (see new Fig. 13), this new factor shows that (in average) the sediment transport is stronger during neap tides than during spring tides. The explanation has been improved, two figures have been added (Fig. 12 and Fig. 13) and more emphasis has been given by including a new section (4.3.2 Tidal correction factor).

Comment 4: To further this, I think an examination of daily tidal fluctuation with the wave height and/or wind speed data might shed some light on the forcing of the bars. For example, the autumn season suggests big forcing but the bars don't see this so much. Could it be that low tide happens during the day, when the winds pick up and blows hard, whereas in late autumn and winter the strong winds begin to coincide with high tide and start to have a stronger effect? There must be a quick and smart way to quantify this. Maybe give high tide a "1", give low tide a "0", and interpolate between them. Then this tidal-like function could be multiplied by the wind or wave signal (like that in Fig 9 or 10) to give a bar-forcing parameter. Something like that?

Following your suggestion we have added a new factor to take into account the area of the bars affected by the wave stirring on each hour. When the tide level is below the lower end of the bars (the system is fully emerged) or above the system (the bars are located at a deep higher than the closure deep), this factor is 0, taking into account that the waves can not stir the sediment from the bars. Only when the tide level allows the surf zone being over the bar system, the factor is higher than 0. The maximum value is reached when the whole surf zone is located over the bars and it is obtained as the percentage of the bar system width covered by the surf zone. So, this factor allows us to take into account:

- The time while the bars are submerged depending on the tidal range.
- The portion of bar system that is affected on each moment, depending on the tidal level and the wave height.

Analysing this factor we can see that it is higher during neap tides and lower during spring tides (see Comment 3).

The methodology followed to compute this new "tidal correction factor" is explained in the new section (section 4.3.2), with the help of the (new) schematic figure Fig. 12. This section also contains the analysis of the behaviour of this factor.

Comment 5: Is there a net transport of sand from the western end, where the finger bars form, to the eastern end, where they decay?

Our analysis suggests that there is a net transport from west to east in our intertidal area, but we do not have field evidence of that.

Comment 6: It is not clear to me where the wind time series came from. What is "theSeaWind"? Are these measured winds?

SeaWind is a wind reanalysis database. It has been obtained by means of an atmospheric dynamic downscaling which has been validated with buoy measurements and satellite data. In the new manuscript, we precise that SeaWind is a database. Additional information can be found in the given reference (Menéndez et al., 2011).

Comment 7: On page 679, line 25 you say that it was checked that 3 points were sufficient to describe the bars. Maybe one more sentence is needed to say how you did this: "We tried using 2 points, 5 points and 7 points to describe the bars and 3 points were found to be sufficient to describe the bar position and orientation." Something like that. Similarly, on page 680 you go on to characterize the bars by choosing 4 points (where those 4 y axes cross). I don't quite understand the two methods, how they are different, and why they are both used. A little more explanation is needed.

Initially the bars are digitized by means of 3 points on each. We tried using 2, 3 and 5 points but 3 points were considered enough to describe the geometry and evolution. To simplify the analysis, once de data is rectified, we made a coordinate system change, that allows us to study the behaviour of the system as a one dimensional problem (along 4 lines) instead of a two dimensional analysis. These explanations have been added in the new section 2.2 (Video imagery and bar detection).

Comment 8: There are many small editorial/English errors. I will communicate with the authors via the editor with those more trivial comments.

We thank the reviewer for her corrections. All grammatical errors have been corrected in the revised manuscript.

Manuscript prepared for Earth Surf. Dynam.
with version 5.7 of the LaTeX class copernicus2.cls.
Date: 17 March 2014

Intertidal finger bars at El Puntal, Bay of Santander, Spain: observation and forcing analysis

E. Pellón, R. Garnier, and R. Medina

Environmental Hydraulics Institute (IH Cantabria), Universidad de Cantabria, Santander, Spain

Correspondence to: E. Pellón (pellone@unican.es) and R. Garnier (garnierr@unican.es)

A system of 15 small-scale finger bars has been observed, by using video imagery, between 23 June 2008 and 2 June 2010. The bar system is located in the intertidal zone of the swell-protected beaches of El Puntal Spit, in the Bay of Santander (Northern coast of Spain). ~~It appears~~ *The bars appear* on a planar beach (slope = ~~1.5 %~~ 0.015) with fine uniform sand (D_{50} = 0.27 mm) and extends 600 m alongshore. The cross-shore span of the bars is determined by the tidal horizontal excursion (between 70 and 130 m). They have an oblique orientation with respect to the low-tide shoreline being ~~up-current oriented with respect to the ebb-flow~~ *down-current oriented with respect to the dominant sand transport computed* (mean angle of 26° from the shore normal). Their mean wavelength is 26 m and their amplitude varies between 10 and 20 cm. The full system slowly migrates to the east ~~(opposite to the ebb-flow)~~ *(sand transport direction)* with a mean speed of 0.06 m day^{-1}, a maximum speed in winter (up to 0.15 m day^{-1}) and a minimum speed in summer. An episode of merging has been identified as bars with larger wavelength seem to migrate ~~slower~~ *more slowly* than shorter bars. ~~Several forcings can act on the bar dynamics being the wind, blowing predominantly from the west, the main candidate to explain the eastward migration of the system.~~ *The wind blows predominantly from the west, generating waves that transport sediment across the bars during high tide periods, which are the main candidate to explain the eastward migration of the system.* In particular, the wind can generate waves of up to 20 cm (root-mean-squared wave height) over a fetch that can reach 4.5 km at high tide. *The astronomical tide seems to be important in the bar dynamics, as the tidal level ~~conditions~~ changes the fetch and also determines the time of exposure of the bars to the surf-zone waves and currents.* Furthermore, the river discharges could act as input of suspended sediment in the bar system and play a role in the bar dynamics.

1 Introduction

Transverse bars are morphological features attached to the shore that appear with a noticeable rhythmicity along the coast of sandy beaches. They have been identified in many types of environments and have been observed with a wide range of characteristics so that a classification of the existing bar systems is necessary. This is not straightforward ~~as~~ *since* these features can be ~~classify with regard to many criterions~~ *classified using many criteria* such as their geometry (length scale, orientation with respect to the shoreline), their dynamics (formation time, migration), or *their* hydromorphological environment. ~~they pertain~~ Alternatively, ~~this~~ *classification* can be made based on the physical processes governing their formation and their dynamics, although ~~this is~~ *these are* sometimes not well understood.

The most documented and observed transverse bar types are probably the "TBR" ("Transverse Bar and Rip") described by Wright and Short (1984), ~~printing a cuspate signature~~ *which impose a cuspate shape* on the shoreline, *sometimes* called megacusps (Thornton et al., 2007). They sometimes appear with an oblique orientation with respect to the shoreline (Lafon et al., 2002; Castelle et al., 2007). The TBR are typically linked to outer morphological patterns, ~~precisely~~ *specifically,* they form due to the onshore migration of a crescentic bar (Ranasinghe et al., 2004; Garnier et al., 2008). They are generally found on open coasts in intermediate wave-dominated beaches, with wavelength (distance between two bars) of 100–500 m, and are associated with the presence of rip currents flowing offshore between two bars. Remarkably, the recent study of Goodfellow and Stephenson (2005) shows that these systems can appear, at smaller scale, in lower energy environment (40 km limited fetch).

Here we will focus on "(transverse) finger bars" that differ from the TBR ~~as~~ *because* they do not emerge from offshore

bathymetric features but they are assumed to form "alone". Moreover, they are not necessarily associated with rip currents. Regarding their geometry, the main difference with the TBR is that ~~they~~ *the finger bars* are long crested, i.e., their cross-shore extent is generally larger than their wavelength. We identify three types of finger bars (Table 1).

1. The first type of finger bars has been identified by Niedoroda and Tanner (1970). We will refer to them as "large scale finger bars" because of their large cross-shore span (~ 1 km). Their wavelength is ~ 100 m and they appear in low energy environments (mean wave height < 0.5 m) on very wide (~ 1 km) beaches with a gentle slope (0.002). They are oriented almost perpendicularly to the shore or with a slight obliquity, in both micro- and macro-tidal environments (Gelfenbaum and Brooks, 2003; Levoy et al., 2013).

2. Although finger bars are often associated with very low wave energy (Wijnberg and Kroon, 2002) a second type of finger bars can be observed in intermediate morphological beach states (Konicki and Holman, 2000; Ribas and Kroon, 2007; *Doeschate et al., 2013*). They coexist, at a smaller wavelength (50–100 m), with other rhythmic morphologies present in the surf-zone, such as with TBR and with crescentic bars. One of the particularities of these "finger bars of intermediate beaches" is that they have an oblique up-current orientation with respect to the mean alongshore current (Ribas et al., ~~2012~~ *2007*).

3. Finally, a third type of finger bars, the "small scale finger bars" appear for very low wave energy in very fetch limited environment (fetch < 10 km), with wavelength of ~ 10 m and a cross-shore span (10–100 m) that depends of the horizontal tidal excursion (Bruner and Smosna, 1989; Garnier et al., 2012). These bars are not strictly normal to the shore (Falqués, 1989; Nordstrom and Jackson, 2012) but seem to be down-current oriented with respect to the *dominant* sand transport (Bruner and Smosna, 1989) ~~that~~ *which* is opposite to the finger bars of intermediate beaches.

The processes of generation and evolution of finger bars are probably different depending on their type, and, particularly, depending on their orientation. ~~Finger bar systems generally migrate in the direction of the sediment transport, but this is not always identified, possibly due to the lack of field data.~~ *It is thought that finger bars generally migrate in the direction of sediment transport, but transport direction is not always identified, possibly due to the lack of field data.* ~~For instance,~~ The theoretical modelling studies of Ribas et al., (2003) and of Garnier et al., (2006) have shown different mechanisms to explain the dynamics of up- and down-current oriented bars by considering forcing due to waves. ~~This has been successfully applied to the finger bars of intermediate beach by Ribas et al., (2012)~~ *Ribas et al., (2012) successfully applied their model to finger bars of an intermediate beach,* based on continuous observations obtained from video imagery. However, the dynamics of finger bars appearing in low energy environments is poorly understood, especially concerning the small scale finger bars ~~as~~ *because* ~~(1) the forcing acting on their dynamics is difficult to determine as, in very limited fetch environment, wind, waves and tidal current, can act with similar intensities,~~ *(1) the forcing is difficult to determine, with forces due to wind, waves and tidal currents all similar in magnitude in very limited fetch environments,* and (2) there is no continuous, *long-term* survey of such systems. Some ~~recent~~ *observation* studies ~~have performed the monitoring of~~ *on* large scale finger bars ~~allowing them to detect mean velocities~~ *have measured mean migration rates* of less than 2 m month^{-1} (Gelfenbaum and Brooks, 2003; Levoy et al., 2013) and maximum speeds of 1 m day^{-1} (Levoy et al., 2013). Concerning small scale finger bars, only the preliminary study of Garnier et al., (2012) gave information on the dynamics of such systems, but, the migration rates detected are overestimated due to strong noise in the data.

The objective of this contribution is to get insight into the dynamics of small scale transverse bars by performing a continuous survey of finger bars detected in the Bay of Santander, Spain, and by analysing the possible forcing ~~that can act in their dynamics~~ *mechanisms.* These finger bars are located in the intertidal zone and the survey is performed by using video images at low tide. Section 2 presents the field site and the dataset obtained by video imagery. Section 3 describes the characteristics and the dynamics of the bar system. Section 4 reports the forcing analysis based essentially on wind data. ~~Section 5 is the conclusion.~~ *The conclusions are listed in Sect. 5.*

2 Field site and video imagery

2.1 Study site

El Puntal spit is part of the natural closure of the Bay of Santander (Fig. 1). This bay is one of the largest estuaries of the northern coast of Spain (Cantabrian Sea). The closure of the bay is composed of two natural formations, the Magdalena peninsula at the north-west, and El Puntal spit at the north-east. This spit is a sand accumulation which extends from east to west along approximately 2.5 km. Historically, more than 50 % of the surface of this bay has been filled in, reducing the tidal prism and changing the morphological equilibrium of El Puntal (Losada et al., 1991) which tends to extend westward. However, for navigation purpose (Medina et al., 2007), the entrance channel is periodically dredged so that the west end of El Puntal is maintained artificially.

There are numerous studies on El Puntal analysing the morphodynamics of the northern face and the west end (Losada et al., 1992; Kroon et al., 2007; Requejo et al., 2008;

Medellín et al., 2008, 2009; Gutiérrez et al., 2011), *but the lower-energy southern face remains unstudied.* ~~but none of them give information about the southern face. The incident energy on each face is very different as~~ The incoming swell from the Cantabrian Sea only reaches the northern face of the spit (Medellín et al., 2008). The southern protected beaches of El Puntal are part of the bay and are located in a low-energy mesotidal environment. The maximum range of the semidiurnal tide is 5 m. Recent hydrodynamic studies (Bidegain et al., 2013) have reported an ebb-oriented mean annual flow of up to 0.1 $m\,s^{-1}$ in the channel at the south of El Puntal. This flow is mainly driven by the (ebb-dominated) tidal current and by the ~~Miera river flow that ends at the east of El Puntal beaches~~ *flow from the Miera river, which enters the bay at the east end of the El Puntal spit.* In the shallower areas the mean flow is much weaker and wind effects can become predominant (Bidegain et al., 2013), especially if we take into account the waves that can be generated over a fetch of up to 4.5 km from the south-west direction. The value of the fetch is highly variable over a tidal cycle due to the numerous intertidal shoals in the bay (Fig. 1b), which can reduce the maximum fetch to 200 m at low tide.

The finger bar system is located in the intertidal zone of the ~~southern beaches~~ *beach on the southern side* of the spit. Aerial images show a system of 15 well developed finger bars that is fully submerged at high tide (Fig. 1c) and fully emerged at low tide (Figs. 1d and 2a). At mid tide the coastline exhibits a cuspate shape (Fig. 2) and processes of wave refraction and wave breaking are observed (Fig. 2c).

The alongshore extent of the bar system is less than 600 m and its mean wavelength (distance between two bars) is about 25 m. The cross-shore extent of the bars is controlled by the tidal horizontal excursion and is larger in the middle of the domain (130 m) than in the lateral sides (70 m). The bars are almost parallel and have an oblique orientation with respect to the low tide coastline, the bar angle with respect to the low-tide shore-normal is about 25° *towards south-east* (0° would correspond to transverse bars). ~~,being up-current oriented with respect to the ebb-flow.~~ The bars are more regularly spaced and parallel in the eastern half of the area, *whilst* the western bars are more irregular, with slight changes in direction and bifurcations (Fig. 1d).

The intertidal beach where the bars appear is planar with a constant slope of approximately ~~1.5 %~~ *0.015.* The offshore boundary of the bars is delimited by a steep slope that ends in the subtidal channel. Sediment sampling has shown the same grain size on bars and troughs with $D_{50} = 0.27$ mm.

2.2 Video imagery *and bar detection*

In the last decades, video monitoring systems are increasingly used to study the shoreline around the world (Holman et al., 1993). To ~~extract~~ *obtain* geometric data of the bar system, the images of the Horus video imagery system were used (www.horusvideo.com). This system is composed of 4 cameras located on the roof of the Hotel Real, 91 m above sea level and 1.5 km from the study area (Fig. 3a). ~~This system was set~~ *The Horus station was established* in 2008 and takes images every 10 min. In the present study only camera 2 has been used (Fig. 3b). The pixel resolution on the study area is variable on the alongshore direction, with values from 4.5 $m\,pixel^{-1}$ to 6.6 $m\,pixel^{-1}$. On the cross-shore direction the resolution is around 0.5 $m\,pixel^{-1}$. One daily image of the bar system has been selected at low tide between 23 June 2008 and 2 June 2010, which is the longest period found without long interruptions in the image database. All the interruptions were of less than 6 consecutive days and were due to technical problems (27 days) and bad meteorological conditions (fog 18 days, strong wind 3 days and bad sharpness 85 days). The geometry of the bars was extracted on 577 days, which is 81 % of the time.

Each bar has been digitised manually by selecting 3 points ~~on each~~ *along the trough:* at the upper part of the beach, at the middle of the bar *system* and at the offshore end of the bar *system* (Fig. 4). ~~It was checked that 3 points per bar is enough to describe their geometry.~~ *We tried using 2 points, 3 points and 5 points to describe the bars and 3 points were found to be sufficient to describe the bar position and orientation.* Finally, the digitised data was rectified by means of 7 Geographic Control Points (GCP), obtaining the geographic coordinates of each digitised point.

The data processed by Garnier et al., (2012) has been reanalysed in order to correct an apparent periodic movement due to sun shadows in the bars. The amplitude of this periodic movement is of the order of the pixel resolution and it has been found that its period is related with the capture times. Furthermore, this apparent movement seems to be a systematic error linked to the different sun positions at low tide during the fortnightly cycle of neap-spring tides, which causes different shadows by the bars and different light reflections in the wet areas. *This light shadowing/reflection also occurs for fixed structures present in the surrounding areas. This allowed us to correct, partially, this spurious movement.*

To better ~~*characterise*~~ *understand the behaviour of the finger bars, the coordinate system of the rectified data has been changed.* ~~*All the measurements of the bar geometry are referenced to*~~ *We defined a new coordinate system,* where the y axis is parallel to the shoreline at low tide (113° from the north, Fig. 4). During a tidal cycle, the mean shoreline position is approximately parallel to the y axis, except at the highest levels of spring tides. *After this transformation, each bar is represented by means of* ~~has been characterised by~~ 4 positions along the $y1$–$y4$ axes (parallel to the y axis) scattered through the intertidal zone, at different levels (see Fig. 4). Each line represents one level along the whole study area (Fig. 5c) and all these lines together are representative of the whole width of the bars.

2.3 3-D geometry

The Horus system captures one image of the study area every 10 min. This means that the path of the shoreline can be observed along the tidal cycle with high frequency. To extract information about the 3-D geometry of the finger bar system, a reconstruction of the intertidal bathymetry of the study area has been performed *by mapping the shoreline from every image.* ~~(Fig. 5a).~~ This must be done ~~at one~~ *on a* day with ~~good meteorological conditions and enough sharpness in all the images during the rising tide.~~ *perfect conditions. The meteorological conditions and image sharpness need to be excellent. Furthermore,* the tide should have the highest range possible, allowing ~~to extract data~~ *the extraction* of a large intertidal region, ~~taking into account that it has to occur completely during the day light.~~ *and this must occur during daylight hours.*

~~After this~~ *On good days,* the shoreline is digitised and rectified on each image. To obtain the bathymetry we assume that the sea level measured at the tide gauge of Santander (less than 2 km away) is the same as the level of the shoreline in the study area. ~~The level with respect to the zero of the harbour of Santander (Z) is associated to each rectified shoreline~~ *The tide level (with respect to the local Santander Harbour datum, Z) at the time of each image is associated with the rectified shoreline from that image,* obtaining ~~the intertidal bathymetry of Fig. 5a.~~ *an intertidal bathymetry.*

2.4 Piecewise regression *of the bar movement*

The method proposed here to ~~detect the main motion~~ *find the time-dependent migration rates* is based on piecewise regressions. *This allows us to focus on the medium term movements rather than on the daily fluctuations.* The time series of the bar position for each bar and each cross-shore position have been decomposed in segments of variable length. The segment length has been set in order to minimise the error between the piecewise signal and the measured positions. ~~For each *bar* signal, the number of segments has been found such that the mean *segment* length corresponds to 70 days (Fig. 6).~~ *After this decomposition, each bar is represented by several segments of different lengths (the segment k has a length of T_k).* For each segment, we can therefore obtain the approximate bar migration *rate* V_k, *which is the migration rate of this bar during the time interval* T_k.

Considering that, at a time t, N segments are obtained (~~for all the bars of the system~~ *where N is the number of bars of the system at this time t, multiplied by four, which is the number of cross-shore positions studied*), the *time-dependent* migration rate of the bar system V_m ~~(Fig. 8)~~ *(which is the average of the speeds, at this time t, of all the bars on all the cross-shore positions)* is computed as:

$$V_m(t) = \sum_{i=1}^{N(t)} \frac{\hat{V}_i(t)}{N(t)}, \text{ where } \hat{V}_i(t) = \begin{cases} V_k, & \text{if } t \in T_k \\ 0, & \text{otherwise} \end{cases} \quad (1)$$

3 Bar characteristics and dynamics

3.1 Bathymetry reconstruction

A bathymetry reconstruction has been done on 12 days with excellent meteorological conditions. Figure 5a shows the bathymetry obtained for 24 June 2008, the day with the best image quality. Cross-shore profiles of this bathymetry (Fig. 5c) show that the bars only appear on the region of the intertidal beach profile which has constant slope of ~~1.5 %~~ *0.015*. The extraction of alongshore profiles from ~~this bathymetry allows~~ *these bathymetries allows* us to measure the amplitude of the bars, which oscillates between 10 and 20 cm. These profiles also show the asymmetry of the bars (Fig. 5b) with steeper slopes on the lee sides (relative to the migration direction), in agreement with previous studies (Gelfenbaum and Brooks, 2003).

3.2 Bar dynamics

During the 2 yr study period the position and geometry of 15 bars have been digitised daily. Figure 6 shows the position of the bar system along the $y3$ axis, *once the digitised data have been corrected, rectified and transformed to the described coordinate system (Fig. 4). Taking into account that the pixel resolution on the study area is of about 5* $\mathrm{m\,pixel^{-1}}$ *on the alongshore direction, the small oscillations visible in Fig. 6 are not deeply analysed, as they could be either physical or measurement errors.* The bar system is persistent in time, appearing in all the observed images with similar geometric characteristics, ~~and extending along the same area~~ but the entire system slowly migrates to the east. As a result of the eastward migration a new bar becomes visible at the west end of the study area (Bar 1, Fig. 6). Although aerial images and the migration of the system suggest that the bars are formed at the west of the study area, the formation area is not included in the present results as it is hidden by the dune (Fig. 5a). At the east end of the area, the last bar decays and slowly disappears. ~~Remarkably, for the whole~~ *In addition, during the* study period, ~~an~~ *only one* episode of merging of two bars into one has been detected, on 28 March 2009 (*bars 5–6,* Fig. 6).

3.2.1 *Time-averaged characteristics* ~~Morphology and Mean motion~~

The digitised and rectified data allow the daily measurement of the bar wavelength. *The bar wavelength is computed as the difference between the positions (on the y_i axis) of two consecutive troughs.* For each bar, the wavelength has been averaged along the complete study period (Fig. 7). The wavelength is approximately constant ~~along the time~~ *for each bar during the study period* (standard deviation σ around 4 m for all bars), ~~and~~ *but* varies between bars, with a minimum of 15 m and a maximum of 36 m. The mean wavelength of the whole bar system is 25.8 m.

Similarly, the ~~mean bar angle with respect to the *x* axis is displayed in Fig. 7. The variability of the angle along the time is low, with σ around 5° for each bar. The angle is variable between bars, with a mean angle of the system of 26.4°, a maximum angle of 34° on the western bar, decreasing to a minimum of 17° on the eastern bar.~~ *variability of the mean bar angle is low, with σ around 5° for each bar. The mean angle of the system , measured from the x axis, is 26.4°, with a maximum angle of 34° at the western end, decreasing to a minimum of 17° at the eastern end (Fig. 7).* The bars are not straight in a top view, so that their angle has also been studied by splitting the bars into 2 parts, the upper (inner) half and the lower (offshore) half. The upper part of all the bars has a lower angle with the shore-normal (mean of the whole system of 23°), while the lower part has higher angles (mean of 31°).

The time series is almost continuous and allows us to compute the ~~velocities of the displacement~~ *time-averaged migration rate of the system, which is obtained by linear regression.* The mean speed of each bar (along the whole study period) is shown in Fig. 7. All the bars of the system slowly migrate to the east, with a mean speed of 6 cm day^{-1} (approximately one wavelength per year). The maximum migration rate is obtained for the bar with the shortest wavelength (8 cm day^{-1}, Bar 5) that merges with the next bar, larger and slower (Bar 6). In general the larger is the wavelength the slower is the migration rate. This is in agreement with previous studies on transverse bars (Garnier et al., 2006).

There are noticeable differences in the dynamics and in the characteristics of the first five bars (western bars) compared with the eastern bars. The western bars (close to the formation zone) are more irregular in shape, with a *larger* mean angle ~~larger~~ (5° larger), ~~and~~ a smaller wavelength (20 m mean) ~~in relation with the larger migration velocity.~~ *and a corresponding higher migration rate.* The eastern bars are well defined and remarkably parallel. Their cross-shore span decreases as they approach the decaying zone.

3.2.2 ~~Time evolution~~ *Time-dependent migration rates*

Each bar signal has been decomposed in 10 segments by means of the piecewise regression described in Sect. 2.4 (Fig. 6). It was found that 10 is the best number to represent the medium term movement of the bar and to filter the daily fluctuations. As we are analysing 2 years of data, the mean segment length is 70 days*. The time-dependent migration rate V_m is computed (Eq. 1).*

The *time-dependent migration rate* of the bar system is not constant along the time *(Fig. 8).* It shows maximum migration rates during winter. The maximum speeds, of about 0.15 m day^{-1}, were reached during the first winter studied (2009), while during the second winter (2010) the maximum speeds are lower than 0.1 m day^{-1}. During summer the system migration is slower, with negative speeds for summer 2008, and migration rates lower than 0.01 m day^{-1} for summer 2009. The negative speeds (i.e. migration to the west) found in summer 2008 can be due to limitations in the computation of V_m that can occur for several reasons. *The accuracy of the piecewise regression is expected to be lower at the beginning and end of the time series, due to the lack of previous/subsequent data. The negative migration rate is obtained for the first segment of the bars only, therefore this result is maybe not realistic.*

4 Forcing analysis

4.1 Forcing candidates

The migration to the east of the bar system indicates a dominant forcing coming from the west. The wind data has been extracted from the SeaWind (Menéndez et al., 2011) reanalysis *database.* Figure 9a shows the wind rose and the time series of the wind speed is displayed in Fig. 9c. The predominant wind is from the west, reaching values of up to 25 m s^{-1}. ~~Meanwhile,~~ The wind from the east is also frequent but less energetic, with speeds lower than 15 m s^{-1}. The mean wind speed is 5 m s^{-1}.

Other studies on transverse bars (Ribas et al., 2003) suggest that waves are the main forcing that controls their dynamics. The study area is protected from the incoming swell (Medellín et al., 2008) and the waves that can act on the bar system are generated locally. According to estuarine studies these wind-waves can have a significant effect in the sediment transport (Green et al., 1997). Here, wind-waves are generated over a maximum fetch of 4.5 km (from the southwest of the study area). ~~At the south, the fetch is highly reduced due to the proximity of the land at less than 1 km. Finally, at the south-east the fetch does not exceed 2 km.~~ *Toward the south and south-east the fetch is reduced by the proximity of land.*

During the survey period, the tidal range oscillates between 1 and 5 m (Fig. 9d). Maximum values of the tidal current in the channel (offshore of the bar system) occur ~~in~~ *during* spring tides with values of up to 0.25 m s^{-1}. In the channel the mean (residual) flow is ebb-oriented, however the residual tidal current is small in the intertidal areas. Computations performed (not shown) with the H2D model (Bárcena et al., 2012) show that the maximum residual current (obtained during spring tides) is lower than 0.01 m s^{-1} in the study area. *Although the residual current is small, the tide can have an effect on the bar dynamics because tidal currents can cause sediment stirring (that is stronger during mid tides), and because of the changes in water level. Firstly, the fetch is strongly dependent on the water level (Green et al., 1997) according to the emersion and submersion of the numerous intertidal shoals during the tidal cycle and this will be taken into account in the wave computations (see Sect. 4.2.1). Secondly, the changes in tidal level affect the time of bar submersion (that is larger during neap tides) and the volume of sand that can be transported (larger if high tide*

coincides with strong winds/waves). This will be taken into account in the sediment transport computations by including the Tidal Correction Factor (see further explanations in Sect. 4.3.2).

Hydrodynamic studies of the Santander Bay have highlighted the effect of the water discharge produced by the Miera River (at the east of the study area) in the annual mean current magnitude in the Bay (Bidegain et al., 2013). Time series of the daily averaged river flow rate are shown in Fig. 9e. Bidegain et al. (2013) have shown that, although the effect of the river is strong in the channel (ebb-oriented flow), the current produced close to the bar system is weak. However, the river discharge can play a role in the bar dynamics as it is linked to a strong sediment supply, that can act as an input of suspended sediment to the bar system.

4.2 Wind *acting on water surface* ~~and wind-waves~~

4.2.1 Wave computation

The wind-waves ~~incoming at the bar~~ *over the* system have been simulated from the wind speed and direction by using the SWAN model (Booij et al., 1999). In the computations, changes in tidal level affecting the fetch have been included. The time series of the wind-waves has been obtained with an interpolation technique based on radial basis functions (RBF), a scheme which is ~~very~~ convenient for scattered and multivariate data (Camus et al., 2011). Results of the root-mean-square (rms) wave height H_{rms} of the waves entering in the bar system are displayed in Fig. 9b (wave rose) and in Fig. 9f (time series of the daily averaged rms wave height). The waves arrive from the west-south-west and south-west ~~during the~~ 65 % of the time, with mean (rms) wave height of 5 cm and period of 1.5 s. During the westward windstorms the waves can reach 20 cm from the west-south-west, with period of 3 s. The other 35 % of the time the waves come from the east-south-east, with wave height lower than 7 cm and period below 1.7 s. The mean wave height from this sector is less than 2 cm with *a period of* 1.2 s.

4.2.2 Wind *stress* vs wind-wave *stress* forcing

The previous studies on transverse bars, where the waves appear ~~clearly~~ to be the main forcing, usually use different indicators to relate the dynamics of the bars with the incident *wave forcing, such that, the alongshore component of the wave energy flux (e.g. Castelle et al., 2007; Price and Ruessink, 2011), or of the wave radiation stress (e.g. Ribas and Kroon, 2007).* ~~forcing (e.g. Ribas and Kroon, 2007; Castelle et al., 2007; Price and Ruessink, 2011).~~

Here, the effect of the local wind is ~~now~~ *also* analysed by computing the alongshore component of the wind *shear stress acting on the water surface* (Fig. 10a and 11a) defined as *(Dean and Dalrymple, 1991)*:

$$T_y = -\rho C_{\mathrm{f}} W^2 \cos\theta_{\mathrm{w}} \tag{2}$$

where ρ *is the water density* ($\rho = 1025\,\mathrm{kg\,m^{-3}}$*),* C_{f} is the friction coefficient, ~~adimensional and~~ equal to 1.2×10^{-6}, W is the wind speed ~~module~~ and θ_{w} is the incoming wind angle (from the shore-normal).

In order to compare the relative effect of the wind *stress* and of the wind waves we define the alongshore wave stress $S_y = S_{xy}/X_{\mathrm{b}}$ (Fig. 10b and 11b). S_{xy} is the alongshore component of the wave radiation stress (Longuet-Higgins and Stewart, 1964) and X_{b} is the surf-zone width. By considering $X_{\mathrm{b}} = H_{rms}/(\beta\,\gamma_{\mathrm{b}})$, we obtain:

$$S_y = \frac{\rho g}{16}\frac{H_{\mathrm{rms}}}{\beta\gamma_{\mathrm{b}}}\sin\theta\cos\theta \tag{3}$$

where g the gravitational acceleration ($g = 9.81\,\mathrm{m\,s^{-2}}$), γ_{b} is the breaking coefficient for irregular waves ($\gamma_{\mathrm{b}} = 0.42$, Thornton and Guza, 1983), β is the beach slope ($\beta = 0.015$) and θ is the offshore wave angle (from the shore-normal). S_y *is an approximation of the term* $\partial S_{xy}/\partial y$ *in the alongshore momentum balance equation, term that is equivalent to* T_y *in the same equation.* ~~allowing us to compare them.~~

Figure 11a and b show the seasonal variability of S_y and T_y respectively. The comparison of *both figures* shows that both forcings have the same order of magnitude and can therefore play a role in the bar dynamics, although S_y is twice ~~larger than~~ *as large as* T_y. ~~The seasonal analysis of the wind stress is the only one that~~ *Only the wind stress seasonal analysis* shows higher energetic conditions in winter 2009 than in winter 2010, ~~according to~~ *in accordance with* the results of the migration rate. *However, the wind stress shows higher energetic conditions in autumn than in winter, while the migration rate shows lower values in autumn 2009 than in winter 2009. The wave stress seasonal analysis shows lower differences between autumns and winters, but with larger values in autumns too.* ~~as the bar migration results suggests.~~

4.3 Sediment transport ~~evaluation~~

The relationship between the bar migration and the alongshore component of the sediment transport is ~~here~~ investigated. ~~Because of the uncertainties in the sediment transport formulations, two different formulas will be used, based on the previous theoretical study of Garnier et al. (2006). We will perform the analysis by considering (1) the simplest sediment transport formulation by assuming that the alongshore component of the sediment transport is proportional to the depth-averaged mean fluid velocity and (2) a more sophisticated~~ We use a formulation based on the Soulsby and Van Rijn formula (Soulsby, 1997). ~~These two formulations have~~ *This formulation has* been used in modelling studies to explain the formation of different kinds of transverse bars (Ribas et al., 2012; Garnier et al., 2006).

4.3.1 Soulsby and Van Rijn ~~(SVR)~~ formula

Here, we assume that the general formulation of the alongshore component of the sediment transport is given by:

$$q = \alpha\,(V_{\text{wave}} + V_{\text{wind}}) \tag{4}$$

where α is the sediment stirring function, V_{wave} is the alongshore component of the wave- and depth-averaged current driven by the wind-waves, and V_{wind} is the alongshore component of the depth-averaged current driven by the local wind.

The alongshore current generated by the wind-waves is approximated from the formula presented by Komar and Inman (1970): ~~It reads~~

$$V_{\text{wave}} = 1.17\,(gH_{\text{rms}})^{0.5}\sin\theta_{\text{b}}\cos\theta_{\text{b}} \tag{5}$$

where θ_{b} is the wave angle at breaking. ~~It~~ *Equation (5)* has been evaluated at the breaking depth defined as $H_{\text{rms}}/\gamma_{\text{b}}$ ($\gamma_{\text{b}} = 0.42$) from the incident wave angle computed with the SWAN model (Sect. 4.1) by using ~~the~~ *Snell's* law and the dispersion relationship.

The alongshore current generated by the wind is computed by assuming the alongshore momentum balance between the wind stress and the bottom friction in case of a quadratic friction law:

$$V_{\text{wind}} = \pm\left|\frac{T_y}{\rho c_{\text{d}}}\right|^{0.5} \tag{6}$$

with c_{d}, the hydrodynamic drag coefficient set as $c_{\text{d}} = 0.005$.

The stirring function *in Eq. (4)* is approximated with the Soulsby and Van Rijn formula (Soulsby, 1997) as:

$$\alpha_{\underline{\text{SVR}}} = \begin{cases} A_{\text{S}}\left(U_{\text{eq}} - U_{\text{crit}}\right)^{2.4} & \text{if } U_{\text{eq}} > U_{\text{crit}} \\ 0 & \text{otherwise} \end{cases} \tag{7}$$

where A_{S} is a coefficient that represents the suspended load and the bed load transport and U_{crit} is the critical velocity above which the sediment can be transported. A_{S} *and* U_{crit} depend essentially on the sediment characteristics and on the water depth (for more details see Soulsby, 1997; Garnier et al., 2006). The equivalent stirring velocity is defined as:

$$U_{\text{eq}} = \left(U_{\text{wind}}^2 + V_{\text{wave}}^2 + \frac{0.018}{C_{\text{d}}}U_{\text{b}}^2\right)^{0.5} \tag{8}$$

where U_{b} is the wave orbital velocity amplitude at the bottom (computed at wave breaking), C_{d} is the morphodynamic drag coefficient computed with the formula of Soulsby (1997) and U_{wind} is the ~~velocity amplitude of the~~ current generated by the wind:

$$U_{\text{wind}} = \left(\frac{C_{\text{f}}}{c_{\text{d}}}W^2\right)^{0.5} \tag{9}$$

4.3.2 Tidal *correction* factor

Although the tidal level variations have been included to compute the incoming wave time series, the sediment transport formula defined in Sect. 4.3.1 does not take into account that the bars can be emerged, and therefore inactive, during part of a tidal cycle. If strong winds and high waves (despite the limited fetch) coincide with the time of emersion, they will have no effect and the effective sediment transport should be zero. Furthermore, the time of submersion depends of the tidal range: during neap tides the bar system is affected by the marine dynamics almost 100 % of the time because the full emersion of the bars occurs only when the tide is at its lowest level (during a short time period); however during spring tides, the active time period is reduced because the tide falls lower and the bars are no longer submerged for a longer time.

These effects have been quantified by means of the tidal correction factor (α_t), ranging from 0 to 1, leading to a new transport formula:

$$q^{\text{t}} = \alpha_t\, q \tag{10}$$

α_t varies every hour, depending on the wave height (H_{rms}) and on the tidal level (η_t). It is computed by using the following formula (see Fig. 12):

$$\alpha_{\text{t}} = \begin{cases} 0 & \text{if } Z_3 < \eta_t \\ \dfrac{Z_3 - \eta_t}{Z_3 - Z_2}\alpha_{\text{t,max}} & \text{if } Z_2 < \eta_t < Z_3 \\ \alpha_{\text{t,max}} & \text{if } Z_1 < \eta_t < Z_2 \\ \dfrac{\eta_t - Z_0}{Z_1 - Z_0}\alpha_{\text{t,max}} & \text{if } Z_0 < \eta_t < Z_1 \\ 0 & \text{if } \eta_t < Z_0 \end{cases} \tag{11}$$

where

$$\alpha_{t,max} = \frac{X_b}{L} = \frac{H_{rms}}{\beta\gamma_b L} \tag{12}$$

with L, the mean cross-shore span of the bars ($L = 100\,\text{m}$). Z_0, Z_1, Z_2, and Z_3 are defined as (see Fig. 12):

$$\begin{cases} Z_0 &= 2.5\ m = \text{Level of the bar lower end} \\ Z_1(t) &= Z_0 + h^*(t) = 2.5 + \gamma_{\text{b}}^{-1}H_{rms}(t) \\ Z_2 &= 3.7\ m = \text{Level of the bar upper end} \\ Z_3(t) &= Z_2 + h^*(t) = 3.7 + \gamma_{\text{b}}^{-1}H_{rms}(t) \end{cases} \tag{13}$$

Z_0 and Z_2 (levels of the bar lower end, and of the bar upper end), are constant and determined from the 3d-geometry (Fig. 5). Z_1 and Z_3 depend on the active depth h^* defined as ($h^* = H_{rms}/\gamma_b$).

To better understand these formulas, let us consider a day with constant wave height. The tidal correction factor is maximum ($\alpha_t = \alpha_{t,max}$) when the maximum depth at the bars is larger than the closure depth ($\eta_t \geq Z_1$) and when the sea

level does not reach the upper end of the bars ($\eta_t \leq Z_2$). This means that the complete surf-zone width is located over the bars. Furthermore, the sediment transport over the bars vanishes if the sea level does not reach the lower end of the bars ($\eta_t \leq Z_0$) and if the minimum water depth at the bars is larger than the closure depth ($\eta_t \geq Z_3$).

From our observations, the tidal factor never reaches one (Fig. 13). $\alpha_t = 1$ would occur for strong stormy conditions: if the surf-zone width is as large as the bar width L ($H_{rms} >$ 0.5), and if it coincides with high tide ($\eta_t = Z_2$). As was expected, Fig. 13 shows that α_t reaches its maximum values during neap tides, preferentially, as the tidal level is close to Z_2 a larger part of the day. During spring tides, the time while the tidal level is between Z_3 and Z_0 is highly reduced, consequently, the tidal factor is, generally, minimum.

4.3.3 Results

Figure 14a shows the results of the sediment transport by using Eq. (4), without the tidal correction. Figure 14b displays the sediment transport by includins the tidal correction factor (Eq. (10)).

In order to analyse the correlation between q and the bar migration rate, we integrate the sediment transport over the time intervals T_k, for each segment that characterises the bar movement (Sect. 3.2.2), and apply Eq. (1) for that sediment transport data, in order to obtain the time-dependent sediment transport time series shown in Fig. 14.

Figure 14a shows that the sediment transport is weaker in spring 2009 than in spring 2010 corresponding to a smaller migration rate. However, the seasonal average of q shows similar values for autumn-winter 2009 and autumn-winter 2010, while the migration rate results show lower values during 2010. The correlation coefficient obtained is r = 0.75.

The addition of the tidal factor improves the results (Fig. 14b) increasing the correlation coefficient to r = 0.8. All correlations obtained are highly significants ($p < 0.001$). The seasonal analysis shows higher values of sediment transport during autumn-winter 2009 than autumn-winter 2010, corresponding with higher time-dependent migration rates during autumn-winter 2009. The sediment transport computed in spring 2009 is lower than in spring 2010, according to the smaller migration rates measured in spring 2009. The time-dependent sediment transport time series of q^t (Fig. 14b) follows the main shape of the measured time-dependent migration rate. The bigger differences are found at the beginning and end of the study period, where none of the models used managed to predict the negative (westward) migration reported during summer 2008, but, as previously mentioned, these negative migration rates can be not realistic.

Figure 9e shows the flow rate of Miera river. This flow rate is bigger during winter 2009 than winter 2010, so the faster migration rate of the bars during this period could be influenced by the river discharge, maybe because it is a source of sediment. However, tests performed by including additional sediment stirring due to the river flow do not show improvement of the results.

5 Conclusions

A small-scale finger bar system has been identified on the intertidal zone of the swell-protected beach of El Puntal Spit in the Bay of Santander (northern coast of Spain). The beach is characterised by a constant slope of ~~1.5 %~~ *0.015* and by uniform sand with $D_{50} = 0.27$ mm. This system appears on the flat intertidal region, which extends over 600 m on the alongshore direction and between 70 m and 130 m on the cross-shore direction (the cross-shore span is determined by the tidal horizontal excursion).

A system of 15 bars has been observed by using the Horus video imaging system during 2 yrs (between 23 June 2008 and 2 June 2010). The bar system has been digitised from daily images at low tide. The data set is almost continuous, with good quality data the 81 % of the time and a maximum continuous period of time without data of 6 days.

The geometric characteristics of the system are almost constant ~~along the~~ *in* time. The mean wavelength of the bar system is 26 m and the bar amplitude is between 10 and 20 cm. Moreover, the bars have an oblique orientation with respect to the low-tide shoreline, with a mean angle of 26° to the east from the shore-normal. We noticed differences in the geometry along the domain: the western bars (first half) are more irregular and have smaller wavelength than the eastern bars (second half).

The full system slowly migrates to the east (against the ebb-flow) with a mean speed of 6 cm day^{-1} that varies between bars. In general, ~~the larger is the wavelength the slower is the migration velocity,~~ *larger wavelength bars migrate more slowly,* in agreement with previous studies ~~on transverse bars.~~ *and satisfying mass conservation.* ~~Remarkably,~~ An episode of merging of two bars has been observed on 28 March 2009: the bar with the smallest wavelength is faster and merges with the next bar. As bars migrate to the east, they form at the west and decay at the east.

A detailed analysis of the bar motion, from a piecewise regression of the bar positions, has shown that bars migrate ~~faster~~ *more quickly* in winter ~~and slower~~ *than* in summer, with maximum migration rates obtained in winter 2009 (0.15 m day^{-1}). Some negative speeds (migration to the west) have been computed (during summer 2008) but this result could be *an effect of the limitations of the piecewise regression at the beginning and end of the time series.*

~~Several forcings can act on the bar dynamics being the wind, blowing predominantly from the west, the main candidate to explain the eastward migration of the system.~~ *The primary forcing mechanism that is acting on the bar dynamics is the wind over the water surface.* Off-shore of the bar system, the mean (annual) flow is ebb-oriented (to the west), because of the Miera River discharge and the astro-

nomical tide. However, in the intertidal zone their effects on the mean flow vanish. There, wind *shear stress* and wind-waves generated over a fetch of up to 4.5 km at high tide, seem to determine the direction of the alongshore transport.

Although residual tidal current is weak, the tide seems to be important in the bar dynamics as the tidal range ~~conditions~~ *changes* the mean (daily) fetch and also the time of exposure of the bars to the marine dynamics. Furthermore, the river discharge could act as input of suspended sediment in the bar system and play a role in the bar dynamics.

The correlation between the bar migration and the alongshore component of the sediment transport has been analysed by using *the Soulsby and Van Rijn formulation. The inclusion of a tidal correction factor improves the results, simulating that the active time depends on the tidal level and the wave height.*

Finally, the bar system is persistent and no formation and no destruction events of the entire system have been observed. Further studies are necessary to understand the formation processes and the full dynamics of these small-scale finger bars. In-situ measurements of the hydrodynamics and sediment concentrations and numerical morphological modelling are essential to deepen ~~on the analysis.~~ *our understanding.* The bar system here has an oblique down-current orientation with respect to the migration direction and has similar characteristics and dynamics to the system described by previous theoretical (modelling) studies that consider the forcing due to waves only *(e.g. Garnier et al., 2006).* However, in our estuarine environment, the dynamics are more complex as different forcings act with the same order of magnitude.

Acknowledgements. The authors thank Puertos del Estado (Spanish Government) for providing tide-gauge data. The work of R. Garnier is supported by the Spanish Government through the "Juan de la Cierva" program. This research is part of the ANIMO (BIA2012-36822) project which is funded by the Spanish government. *The authors thank the editor G. Coco, and the referees F. Ribas and E. Gallagher for their useful comments.*

References

Bárcena, J. F., García, A., García, J., Álvarez, C., and Revilla, J. A.: Surface analysis of free surface and velocity to changes in river flow and tidal amplitude on a shallow mesotidal estuary: an application in Suances Estuary (Nothern Spain), J. Hydrol., 14, 301–318, 2012.

Bidegain, G., Bárcena, J. F., García, A., and Juanes, J. A.: LARVAHS: predicting clam larval dispersal and recruitment using habitat suitability-based particle tracking mode, Ecol. Model., 268, 78–92, 2013.

Booij, N., Ris, R. C., and Holthuijsen, L. H.: A third-generation wave model for coastal regions, Part I, Model description and validation, J. Geophys. Res., 104, 7649–7666, 1999.

Bruner, K. R. and Smosna, R. A.: The movement and stabilization of beach sand on transverse bars, Assateague Island, Virginia, J. Coastal Res., 5, 593–601, 1989.

Camus, P., Méndez, F. J., and Medina, R.: A hybrid efficient method to downscale wave climate to coastal areas, Coast. Eng. 58, 851–862, 2011.

Castelle, B., Bonneton, P., Dupuis, H., and Senechal, N.: Double bar beach dynamics on the high-energy meso-macrotidal French Aquitanian coast: a review, Mar. Geol., 245, 141–159, 2007.

Dean, R. G. and Dalrymple, R. A.: Water wave mechanics for engineers and scientists, World Scientific, 157–158, 1991.

Doeschate, A., Ribas, F., de Swart, H., Ruessink, G., and Calvete,D.: Observations and modeling of transverse finger bars, Proc. Coastal Dynamics, 208, 2013.

Falqués, A.: Formación de topografía rítmica en el Delta del Ebro, Revista de Geofísica, 45, 143–156, 1989.

Galal, E. M. and Takewaka, S.: Longshore migration of shoreline mega-cusps observed with x-band radar, Coast. Eng. J., 50, 247–276, 2008.

Garnier, R., Calvete, D., Falqués, A., and Caballeria, M.: Generation and nonlinear evolution of shore-oblique/transverse sand bars, J. Fluid Mech., 567, 327–360, 2006.

Garnier, R., Calvete, D., Falqués, A., and Dodd, N.: Modelling the formation and the long-term behavior of rip channel systems from the deformation of a longshore bar, J. Geophys. Res., 113, C07053, doi:10.1029/2007JC004632, 2008.

Garnier, R., Medina, R., Pellón, E., Falqués, A., and Turki, I.: Intertidal finger bars at El Puntal spit, bay of Santander, Spain, Proceedings of the 33rd Conference on Coastal Engineering, ASCE, Santander, Spain, 1–8, 2012.

Gelfenbaum, G. and Brooks, G. R.: The morphology and migration of transverse bars off the west-central Florida coast, Mar. Geol., 200, 273–289, 2003.

Goodfellow, B. W. and Stephenson, W. J.: Beach morphodynamics in a strong-wind bay: a low-energy environment?, Mar. Geol., 214, 101–116, 2005.

Gutiérrez, O., González, M., and Medina, R.: A methodology to study beach morphodynamics based on self-organizing maps and digital images, Proceedings of the Coastal Sediments 2011, World Scientific, 2453–2464, 2011.

Green, M. O., Black, K. P., and Amos, C. L.: Control of estuarine sediment dynamics by interactions between currents and waves at several scales, Mar. Geol., 144, 97–116, 1997.

Holman, R. A., Sallenger Jr., A. H., Lippmann, T. C. D., and Haines, J. W.: The application of video image processing to the study of nearshore processes, Oceanography, 6, 78–85, 1993.

Komar, P. and Inman, D.: Longshore sand transport on beaches, J. Geophys. Res., 75, 5514–5527, 1970.

Konicki, K. M. and Holman, R. A.: The statistics and kinematics of transverse sand bars on an open coast, Mar. Geol., 169, 69–101, 2000.

Kroon, A., Davidson, M. A., Aarninkhof, S. G. J., Archetti, R., Armaroli, C., González, M., Medri, S., Osorio, A., Aagaard, T., Holman, R. A., and Spanhoff, R.: Application of remote sensing video systems to coastline management problems, Coast. Eng., 54, 493–505, 2007.

Lafon, V., Dupuis, H., Howa, H., and Froidefond, J. M.: Determining ridge and runnel longshore migration rate using spot imagery, Oceanol. Acta, 25, 149–158, 2002.

Levoy, F., Anthony, E. J., Monfort, O., Robin, N., and Bretel, P.: Formation and migration of transverse bars along a tidal sandy coast deduced from multi-temporal Lidar datasets, Mar. Geol.,

342, 39–52, 2013.

Longuet-Higgins, M. S. and Stewart, R. W.: Radiation stresses in water waves: a physical discussion with applications, Deep-Sea Res., 11, 529–562, 1964.

Losada, M. A., Medina, R., Vidal, C., and Roldan, A.: Historical evolution and morphological analysis of "EI Puntal" Spit, Santander (Spain), J. Coastal Res., 7, 711–722, 1991.

Losada, M. A., Medina, R., Vidal, C., and Losada, I. J.: Temporal and spatial cross-shore distributions of sediment at "El Puntal" spit, Santander, Spain, Coast. Eng., 1992, Proceedings of the Twenty-Third International Conference, 2251–2264, 1992.

Medellín, G., Medina, R., Falqués A., and González, M.: Coastline sand waves on a low-energy beach at "El Puntal" spit, Spain, Mar. Geol., 250, 143–156, 2008.

Medellín, G., Falqués A., Medina, R., and González, M.: Coastline sand waves on a low-energy beach at El Puntal spit, Spain: linear stability analysis, J. Geophys. Res., 114, C03022, doi:10.1029/2007JC004426, 2009.

Medina, R., Marino-Tapia, I., Osorio, A., Davidson, M., and Martín F. L.: Management of dynamic navigational channels using video techniques, Coast. Eng., 54, 523–537, 2007.

Menéndez, M., Tomás, A., Camus, P., García-Díez, M., Fita, L., Fernández, J., Méndez, F. J., and Losada, I. J.: A methodology to evaluate regional-scale offshore wind energy resources, OCEANS'11 IEEE Santander Conference, Spain, 1–9, 2011.

Niedoroda, A. W. and Tanner, W. F.: Preliminary study of transverse bars, Mar. Geol., 9, 41–62, 1970.

Nordstrom, K. F. and Jackson, N. L.: Physical processes and landforms on beaches in short fetch environments in estuaries, small lakes and reservoirs: a review, Earth-Sci. Rev., 111, 232–247, 2012.

Price, T. D. and Ruessink, B. G.: State dynamics of a double sandbar system, Cont. Shelf. Res., 31, 659–674, 2011.

Ranasinghe, R., Symonds, G., Black, K., and Holman, R.: Morphodynamics of intermediate beaches: a video imaging and numerical modelling study, Coast. Eng., 51, 629–655, 2004.

Requejo, S., Medina, R., and González, M.: Development of a medium-long term beach evolution model, Coast. Eng., 55, 1074–1088, 2008.

Ribas, F. and Kroon, A.: Characteristics and dynamics of surfzone transverse finger bars, J. Geophys. Res., 112, F03028, doi:10.1029/2006JF000685, 2007.

Ribas, F., Falqués, A., and Montoto, A.: Nearshore oblique sand bars, J. Geophys. Res., 108, C43119, doi:10.1029/2001JC000985, 2003.

Ribas, F., de Swart, H. E., Calvete, D., and Falqués, A.: Modeling and analyzing observed transverse sand bars in the surf zone, J. Geophys. Res., 117, F02013, doi:10.1029/2011JF002158, 2012.

Soulsby, R. L.: Dynamics of Marine Sands, Thomas Telford, London, UK, 1997.

Thornton, B. and Guza, R. T.: Transformation of wave height distribution, J. Geophys. Res., 88, 5925–5938, 1983.

Thornton, E. B., MacMahan, J., and Sallenger Jr., A. H.: Rip currents, mega-cusps, and eroding dunes, Mar. Geol., 240, 151–167, 2007.

van Enckevort, I. M. J., Ruessink, B. G., Coco, G., Suzuki, K., Turner, I. L., Plant, N. G., and Holman, R. A.: Observations of nearshore crescentic sandbars, J. Geophys. Res., 109, C06028, doi:10.1029/2003JC002214, 2004.

Wijnberg, K. M. and Kroon, A.: Barred beaches, Geomorphology, 48, 103–120, 2002.

Wright, L. D., Short, A. D.: Morphodynamic variability of surf zones and beaches: a synthesis, Mar. Geol., 56, 93–118, 1984.

Table 1. Transverse bar types and main characteristics.

Type	Beach type	Mean wave height (m)	Bar wave-length (m)	Cross-shore span (m)	Bar orientation	Migration rate[a] ($m\,day^{-1}$)	Reference of observed bars
TBR (Trans-verse Bars and Rips)	Inter-mediate wave-dominated beaches	> 0.5	100–500	< 150	Normal, Oblique	5[b]	Wright and Short (1984) Lafon et al. (2002) Ranasinghe et al. (2004) Goodfellow and Stephenson (2005)[c] Castelle et al. (2007) Thornton et al. (2007)
Large Scale Finger Bars	Low energy beaches, wide (~ 1 km) with gentle slope (0.002)	< 0.5	~ 100	~ 1000	Normal or slightly oblique	1	Niederoda and Tanner (1970) Gelfenbaum and Brooks (2003) Levoy et al. (2013)
Finger Bars of Inter-mediate Beaches	Intermediate wave-dominated beaches	> 0.5	50–100	< 100	Oblique up-current oriented	40	Konicki and Holman (2000) Ribas and Kroon (2007) *Doeschate et al. (2013)*
Small Scale Finger Bars	Very fetch – limited (< 10 km)	< 0.1	< 50	< 100	Oblique down-current oriented	Lack of data	Falqués (1989) Bruner and Smosna (1989) Nordstrom and Jackson (2012) Garnier et al. (2012) Present study

[a] The values given for the migration rates are the maximum alongshore velocities detected.
[b] Some studies have detected alongshore migration rates of crescentic bars (van Enckevort et al., 2004) and of mega-cusps (Galal and Takewaka, 2008) much larger (~ 50 $m\,day^{-1}$) but these systems are not clearly coupled with TBR.
[c] Identify smaller scale TBR in low energy environment.

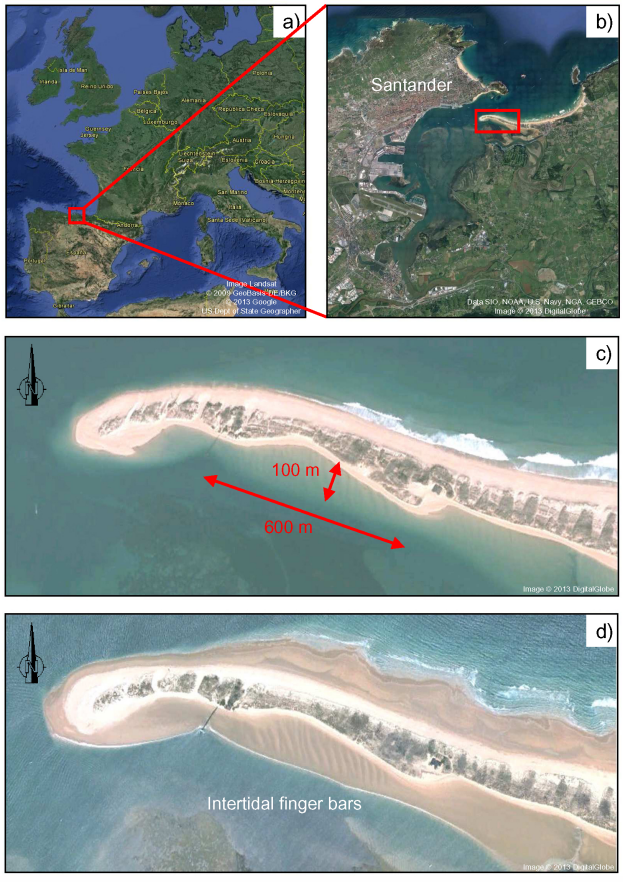

Figure 1. **(a)** Location of Santander, **(b)** Map of the bay, **(c)** El Puntal at high tide, **(d)** El Puntal at low tide. Images from Google Earth.

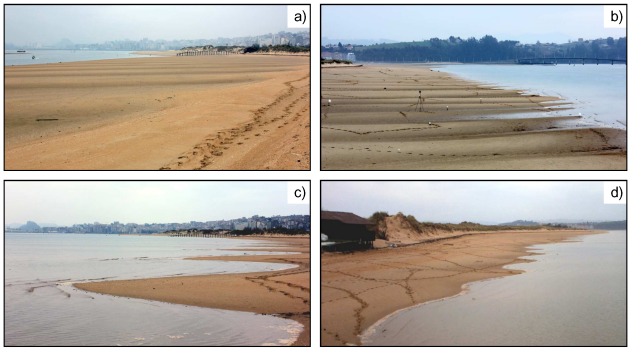

Figure 2. Photos at **(a, b)** low tide, **(c, d)** rising tide. Pictures taken from the east end of the study area **(a, c)**, and from the west end **(b, d)**. Capture date: 25 February 2012.

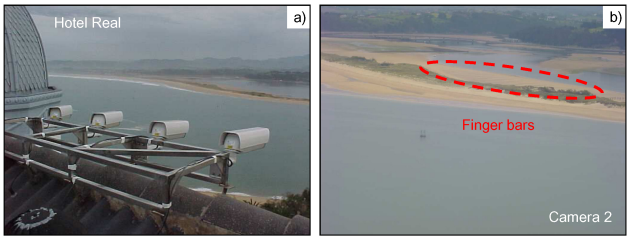

Figure 3. Horus video system. **(a)** Cameras at the roof of the Hotel Real, **(b)** Image taken by camera 2.

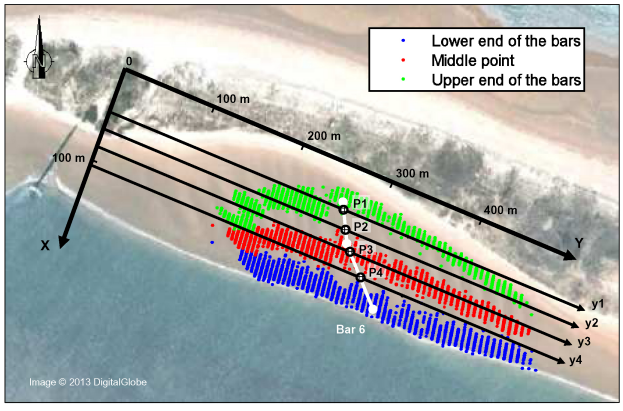

Figure 4. Coordinate system and bar digitisation. The x and y axes stand for the cross-shore and the alongshore direction, respectively. The colour points represent the digitised data (each bar is represented by 3 points); blue, red and green are the outer, the middle and the inner points of the bars, respectively. The bar positions (P1–P4) are defined along the $y1$–$y4$ axes (see positions of Bar 6, in white).

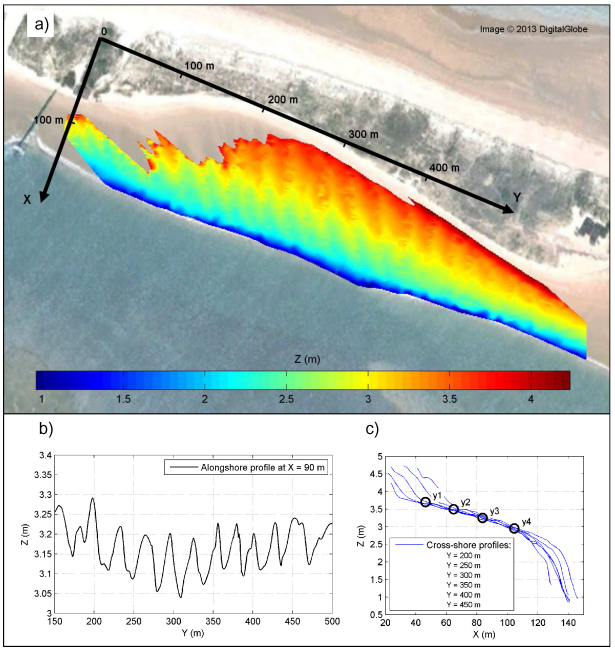

Figure 5. **(a)** Bathymetry reconstruction *with videoed shoreline positions during rising tide* (24 June 2008). The north-west area without data is the shadowed area by the dune, from the point of view of the camera. **(b)** Alongshore profile of the bed level. **(c)** Cross-shore profiles of the bed level and cross-shore positions of the $y1$–$y4$ axes.

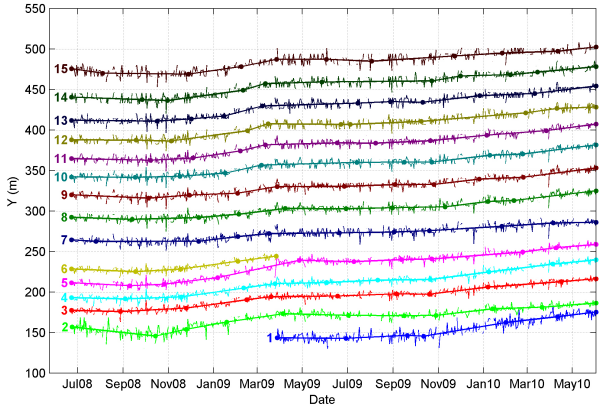

Figure 6. Evolution of the bar system. Time series of the bar position along the $y3$ axis. The thin discontinuous lines represent the measured position. The thick segments represent the piecewise regression of the measured position. The number at the left side of each lines indicates the bar number.

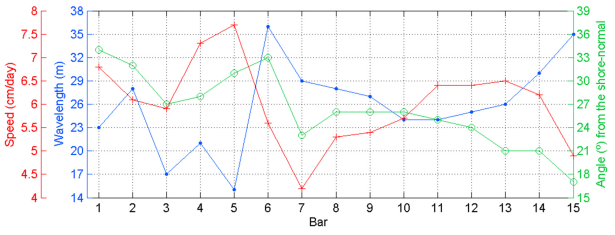

Figure 7. Mean wavelength, angle and *time-averaged migration rate* ~~speed (averaged on time)~~ of each bar. The bar angles are measured from the shore-normal to the east. Positive values of the bar speeds represent movements of the bars to the east.

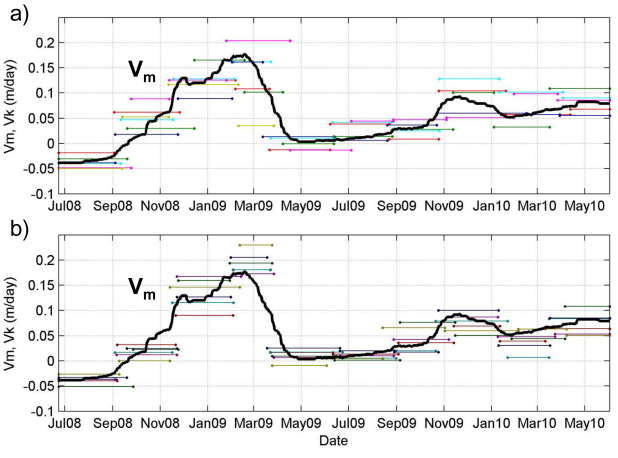

Figure 8. *Time-dependent migration rate of the transverse bars. V_m (thick-black line), time-dependent migration rate of the bar system. V_k (colour lines), individual bar migration rate (the colours correspond to Fig. 6).* ***(a)*** *V_k for bars 3–8.* ***(b)*** *V_k for bars 9–14.* ~~Migration speed Time-varying migration rate of the transverse bars. V_m (thick-black line), migration velocity of the bar system. V_k (colour lines), individual bar migration velocity (the colours correspond to Fig. 6). **(a)** V_k for bars 3–8. **(b)** V_k for bars 9–11.~~

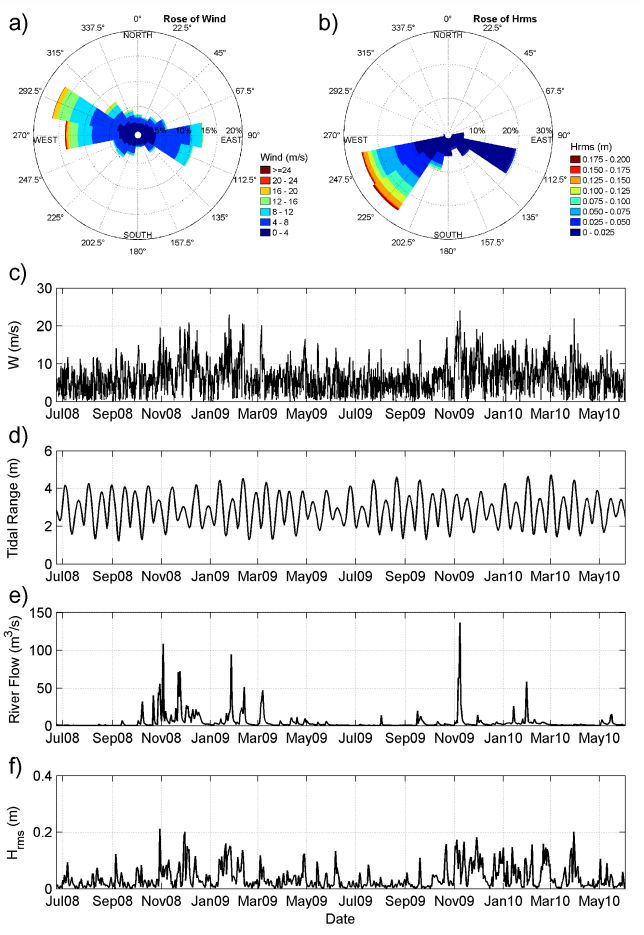

Figure 9. **(a)** Wind rose. **(b)** Wave rose. **(c–f)** Time series of the **(c)** wind speed W, and the daily averaged **(d)** tidal range, **(e)** river flow rate, **(f)** root-mean-square wave height of the wind waves H_{rms}.

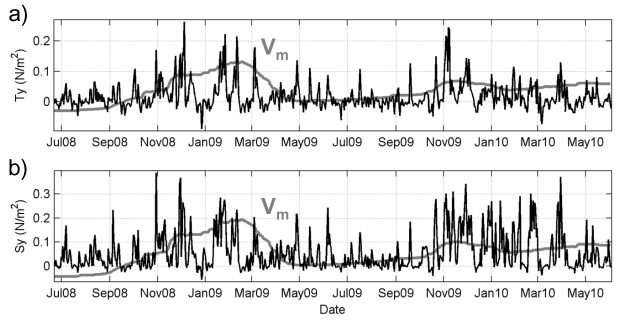

Figure 10. Time series of the daily averaged ***(a)*** *alongshore wind stress (T_y, black) and* ***(b)*** *alongshore wave stress (S_y, black).* ~~wave power (P, black) and alongshore wave power (P_y, red), **(b)** alongshore component of the wave radiation stress (S_{xy}, black), and **(c)** alongshore wind stress (T_y, black).~~ The grey lines represent the behaviour of the bar migration rate V_{m} that has been redimensionalised with the above variables.

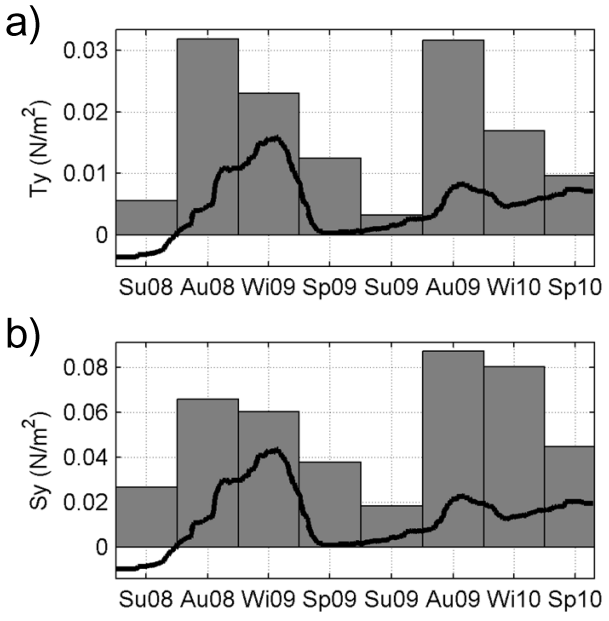

Figure 11. Seasonal variability of ***(a)*** *alongshore wind stress (T_y) and* ***(b)*** *alongshore wave stress (S_y).* ~~**(a)** wave power (P, grey) and alongshore wave power (P_y, red), **(b)** alongshore component of the wave radiation stress (S_{xy}), **(c)** alongshore wave stress (S_y), and **(d)** alongshore wind stress (T_y).~~ The black lines represent the behaviour of the bar migration rate V_{m} that has been redimensionalised with the above variables. The bottom axes indicate the seasons, from summer 2008 to spring 2010.

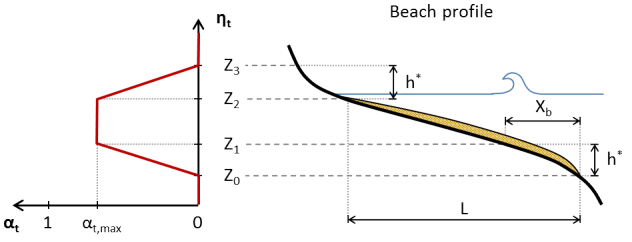

Figure 12. *Parameters for the calculation of the tidal correction factor (α_t). It depends on the tidal level (η_t), the mean cross-shore span of the bars (L), the active depth (h^*), the surf-zone width (X_b), the level of the bar lower end (Z_0), of the bar upper end (Z_2) and the levels Z_1 and Z_3 which vary with the wave height (H_{rms}).*

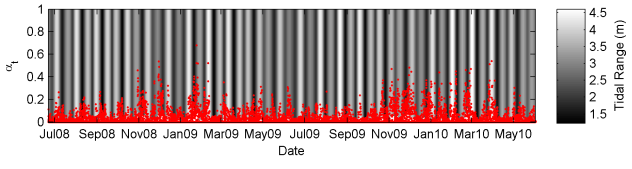

Figure 13. *Time series of: the tidal correction factor α_t (red dots); and the tidal range (greyscale, vertical bars).*

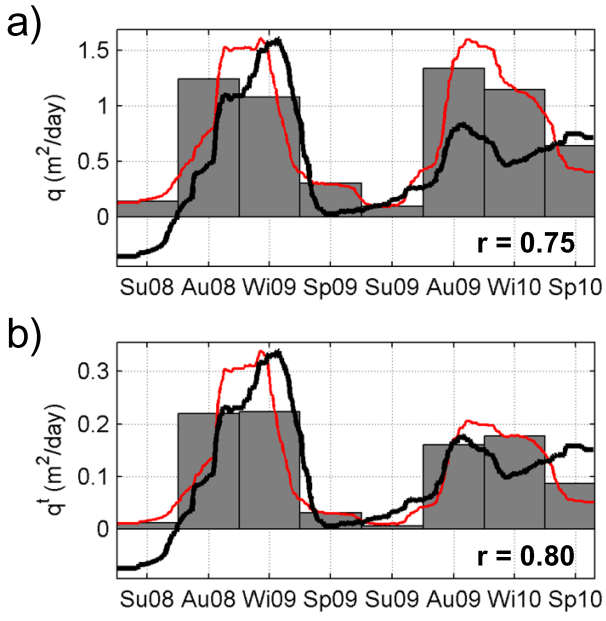

Figure 14. Sediment transport evaluation. Analysis of ***(a)*** *alongshore component of sediment transport q (without tidal correction), and* ***(b)*** q^t *(with tidal correction). The grey areas show the seasonal variability and the red lines the time-dependent sediment transport time series (obtained by averaging over the T_k intervals). The black lines represent the behaviour of the bar migration rate V_m that has been redimensionalised with the above variables. The correlation coefficient of both lines is shown in the bottom right corner. The bottom axes indicate the seasons, from summer 2008 to spring 2010.* ~~(from top to bottom): **(a, b)** alongshore current driven by the wind-waves (V_{wave}), **(c, d)** alongshore current driven by the wind (V_{wind}), **(e, f)** alongshore component of the Soulsby and Van Rijn (SVR) formula (q_{SVR}), and **(g, h)** SVR formula with tidal correction (q^t_{SVR}). Left **(a, c, e, g)**: seasonal variability (see caption of Fig. 11). Right **(b, d, f, h)**: scatter plot and linear regression between the above variables and the bar migration velocity (V_k).~~